Available online at www.sciencedirect.com

ScienceDirect

Procedia Engineering 2 (2010) 1421–1430

Procedia Engineering

www.elsevier.com/locate/procedia

Fatigue 2010

Plastic deformation behavior of Cu thin films during fatigue testing

Chung-Youb Kim[a,]*, Ji-Ho Song[b], Yun Hwangbo[b], Heung-Soo Shim[b]

[a]*Division of Mechanical and Automotive Engineering, Chonnam National University, San 96-1, Dunduck-dong, Yosu, Chonnam, 550-749, Korea*

[b]*Department of Mechanical Engineering, Korea Advanced Institute of Science and Technology 373-1, Guseong-dong, Yuseong-gu, Daejeon, 305-701, Korea*

[c]*Department of Nano Convergence and manufacturing Systems Research Division 104 Sinseongno, Yuseong-gu, Daejeon 305-343, Korea,*

Received 8 March 2010; revised 9 March 2010; accepted 15 March 2010

Abstract

Plastic deformation behavior of electrodeposited copper films with thickness of 12 μm was investigated by using a testing system employed an electro-dynamic actuator. During the fatigue tests, cyclic plastic strain and ratcheting strain were measured continuously with high precision by using the capacitance extensometer. Since the displacement gage is stable and its response is so fast, the deformation can be measured in real time during fatigue tests as well as tensile tests. The cyclic plastic strain range and monotonic plastic strain increase with loading cycles and they are similar to the conventional creep curve. The monotonic plastic strain at fracture is nearly constant, irrespective of mean stress, indicating that the monotonic plastic strain can be used as an indicator of damage. Based on these results, a prediction method for the monotonic plastic strain is proposed. It could be found from the prediction results that the monotonic plastic strain is well predicted.

Keywords: Electrodeposited copper film; Fatigue test; Mean stress effect; Cyclic plastic strain; Ratcheting strain;

1. Introduction

The fatigue properties as well as mechanical properties of thin films widely used in electronic devices are essential to evaluate performance and reliability of the devices, and it is well known that mechanical properties of thin films are different from those of bulk materials and vary depending on fabrication method and film thickness [1-5]. Accordingly, a number of studies on the mechanical behavior of thin films have been reported by many investigators [6-10], while the studies of fatigue behavior of thin films [1,11-16] are not so much due to difficulties in performing fatigue tests. Fatigue testing of thin films is usually performed under tension–tension loading conditions since compressive load cannot apply to thin film, so that assessment of the tensile mean stress effect on fatigue life is very important. However, there are only two investigations discussing the effect on fatigue life, by Schweiger and Kraft [14], and by Park et al. [15]. Schweiger and Kraft performed fatigue tests, varying the mean stress only for a very limited range of stress amplitudes on a 0.6 μm thick Ag film and concluded that the data could be described by Morrow's law. However, their conclusion was based on very limited data. Park et al. tested a 15 μm

* Corresponding author. Tel.: +82-61-659-3222; fax: +82-61-659-3229.
E-mail address: kimcy@chonnam.ac.kr.

1877-7058
doi:10.1016/j.proeng.2010.03.154

thick electrodeposited copper film for a relatively wide range of stress amplitudes at two levels of mean stresses and reported that the modified Goodman equation can consider well the mean stress effect. The tensile mean stress is very likely to lead to occurrence of the so-called ratcheting deformation that may influence fatigue life. There is little work [11,15] on the ratcheting behavior of thin films. Hong and Weil [11] reported only the fatigue fracture strain in low cycle fatigue of thin copper foils and Park et al. [28] observed the ratcheting deformation during high cycle fatigue tests of a thin copper film. The authors [16] also studied the mechanical and fatigue behavior of a copper film which can be easily obtained and tested under free standing conditions. In the work, behavior of cyclic plastic deformation and ratcheting deformation were investigated in detail, performing fatigue tests and tensile tests were also carried out to obtain the reference mechanical properties of the testing copper film. In this study, effect of mean stress and plastic deformation behavior of copper films during cyclic loading was discussed based on the previous work [16] and a prediction method of the monotonic plastic strain behavior was proposed.

2. Experimental details

2.1. Material and specimen

The material used is an electrodeposited copper foil of 12 μm thickness fabricated by Furukawa Circuit Foil Co., Ltd, which is mainly used for flexible multilayer wiring boards. Fig.1 shows surface images of the foil by a scanning electron microscope (SEM). Owing to the manufacturing process, the roughness of the both surfaces is very different on its two surfaces, the drum side and the outer side surfaces: The drum side surface which is peeled off from the cathode drum is called ‘shiny side’ and is lustrous and smooth and has a longitudinally liny pattern, as shown in Fig. 1(a). The outer side surface which shows the end of the crystals is called ‘matte side’ and is lusterless and very bumpy, as shown in Fig. 1(b). For both surfaces, the grain size varies in a wide range and the grain shape is also significantly varied from grain to grain. The grain of the matte surface is larger than that of the shiny surface and the averaged grain size is about 0.6 μm. Fig. 2 shows schematic configurations of the specimen fabricated by etching. The specimen is a dog-bone type, which has a gage section 0.5 mm wide by 5 mm long.

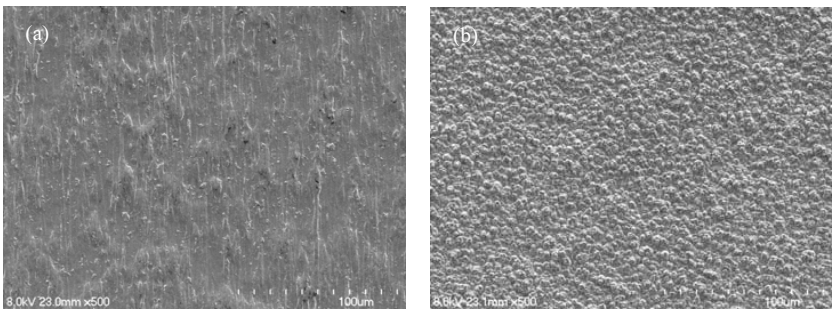

Fig. 1 SEM images of (a) shiny, and (b) matt surface.

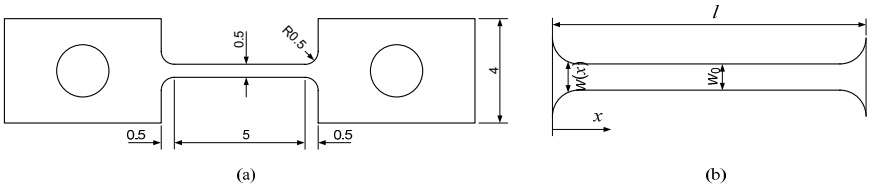

Fig. 2 Schematic configurations of the specimen (unit: mm)

2.2. Testing system

Fig. 3(a) shows the testing system used. The testing machine is a home-made, electro-dynamic, vertical-type axial loading one of small capacity (5 N), which is an improved model of the previous developed one [17]. The load is measured by a commercial load cell (Sentotec Ltd.) of strain gage type with a load capacity of 2.45 N. The displacement of specimen is measured by a home-made, capacitive extensometer (sensitivity: 11.3 mV/μm, linearity: 0.13 %) shown in Fig. 3(b), which is an improved model of the previous developed one [17]. The capacitive type gage is a kind of non-contact measurement method with high resolution. The capacitive extensometer consists of a frame, an upper and lower electrode, and a ground electrode. The frame supporting two electrodes is fastened to the upper grip of the testing machine and the ground electrode connected to the lower grip is initially located at the middle of the two electrodes, so that the extensometer measures the relative displacement between the two grips. The response of the capacitive gage is so fast that real time measurement is possible without any restriction on the testing frequency.

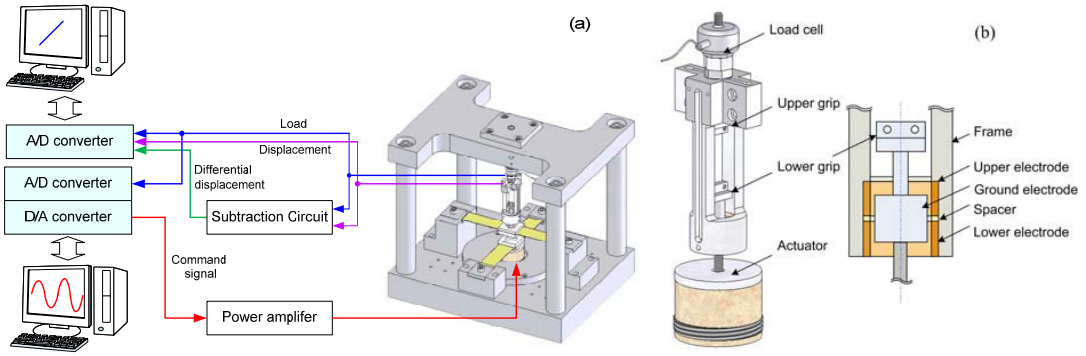

Fig. 3 Schematic configurations of (a) testing system and (b) capacitance extensometer

Monotonic tensile tests were performed at initial loading rate of 5 MPa/s. Fatigue tests were conducted at a frequency of 13 Hz under load control. The fatigue load signal is monitored cycle by cycle and if the mean load or the load amplitude is not within an allowable error band (±0.1 %), the command input signal to the testing machine is adjusted by a control program in a computer. Both the mean load and the load amplitude were successfully controlled within the maximum error of about 0.25 %.

2.3. Calculation of strain

The capacitive extensometer measures the relative displacement between the upper and lower grips, so that the measured displacement involves not only the deformation component of the gage section but also the deformation component of the two fillet areas. Therefore, in order to calculate the strain of the specimen from the displacement data obtained by the capacitive extensometer, the displacement on the fillet portion of specimen should be taken into account, and in this study, is considered by introducing equivalent gage lengths l_{eq}. The equivalent gage lengths for the elastic and plastic deformation, $l_{eq.e}$ and $l_{eq.p}$, were calculated because the equivalent gage length is different depending on elastic or plastic deformation [16].

When the specimen shown in Fig. 2(b) deforms elastically, the elastic displacement δ_e for the total length l which includes the fillet portions of specimen can be calculated as

$$\delta_e = \int_0^l \varepsilon \, dx = \int_0^l \frac{\sigma}{E} dx = \frac{P}{Et} \int_0^l \frac{1}{w(x)} dx \tag{1}$$

where E is the elastic modulus, P is load, A is cross-sectional area, and t and $w(x)$ are the thickness and width of specimen, respectively. Since the elastic strain on the gage length, ε_{0e}, is $P/(Etw_0)$, Eq.(1) will be

$$\delta_e = \varepsilon_{0e} w_0 \int_0^l \frac{1}{w(x)}\,dx \quad \therefore \varepsilon_{0e} = \delta_e / \int_0^l \frac{w_0}{w(x)}\,dx . \tag{2}$$

If we define the elastic equivalent gage length as

$$l_{eq.e} = \int_0^l \frac{w_0}{w(x)}\,dx , \tag{3}$$

the elastic strain on the gage length can be calculated from the elastic displacement for the length l as

$$\varepsilon_{0e} = \delta_e / l_{eq.e} . \tag{4}$$

On the other hand, if the stress-plastic strain curve is represented as

$$\sigma = k\varepsilon_p^n , \tag{5}$$

the plastic displacement δ_p can be obtained as

$$\delta_p = \int_0^l \varepsilon_p\,dx = \int_0^l (\sigma/k)^{1/n}\,dx = (P/kt)^{1/n} \int_0^l \{1/w(x)\}^{1/n}\,dx , \tag{6}$$

where k and n are the strength coefficient and strain-hardening exponent, respectively. Because the plastic strain on the gage length, ε_{0p}, is $(\sigma/k)^{1/n}$, the plastic equivalent gage length can be obtained as

$$\varepsilon_{0p} = \delta_p / l_{eq.p}, \quad l_{eq.p} = \int_0^l \{w_0 / w(x)\}^{1/n}\,dx . \tag{7}$$

Using the elastic and plastic equivalent gage length, the elastic and plastic strains on the gage length of specimen can be easily calculated from the output of the extensometer. For the specimen shown in Fig. 2(a) where the gage length is 5 mm and the total length l is 6 mm, the elastic equivalent gage length is $l_{eq.e}$ = 5.76 mm. The value of plastic equivalent gage length varies depending on strain-hardening exponent n. The strain-hardening exponent n is about 0.1 as described later, so the elastic equivalent gage length of $l_{eq.p}$ = 5.28 mm was obtained from Eq. (7).

3. Experimental results

3.1. Tensile test results

Fig. 4 shows stress-strain curves, *S*-*e*, obtained from the monotonic tensile tests, where the strain was calculated using the elastic equivalent gage length $l_{eq.e}$ described in the previous section, to conveniently calculate the elastic modulus of material. The elastic modulus is about 85 GPa. The 0.2 % offset and 0.5 % extension-under-load yield strengths were 235 and 234 MPa, respectively. The two yield strengths are almost the same. This may mean that the yield strength of thin films can be determined easily by the 0.5 % extension-under-load instead of 0.2 % offset yield strength. Since the initial loading portions of the stress-strain curves is non-linear and the slope of the liner portion varied widely, it is obscure and difficult to determine the offset yield stress which is usually used to identify the yield strength of a material. The tensile strength is 317 MPa. The elongation is 13.2 % for a gage length of 5 mm of the specimen shown in Fig. 2(a). The strain-hardening exponent n is obtained by repeating computation along with the plastic equivalent gage length $l_{eq.p}$ described in the previous section, till their values converge. The value of n is

0.097 nearly close to 0.1. It has been reported [2,18] that the elastic modulus of copper thin films is significantly influenced by fabrication method, film thickness and microstructure, and is below the bulk published values. For electrodeposited copper films, the reported values were 92 GPa (35 μm thickness) and 102 GPa (105 μm thickness) by Klein et al. [2] and 72 GPa (15 μm thickness) by Park et al. [15]. The value of 94 GPa is the elastic modulus measured under elastically cyclic loading. The value under cyclic loading is about 11% higher than that under tensile testing. The value of elastic modulus obtained under cyclic loading can be considered to be more reliable than that under tensile testing.

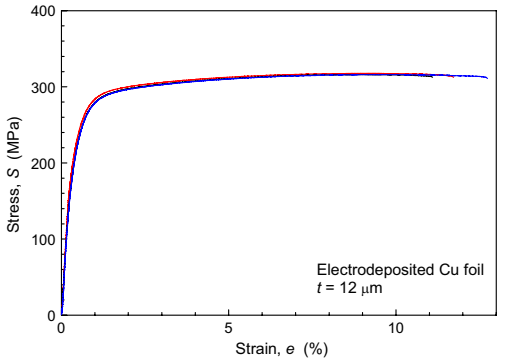

Fig. 4 Stress-strain curve

3.2. Fatigue test results

3.2.1. S-N curve

Fig. 5(a) shows fatigue test results obtained at mean stresses of S_m= 190, 200, 210, and 220 MPa. The range of mean stress corresponds to 0.60~0.69S_u and 0.82~0.95S_y and all the maximum stress S_{max} is greater than the yield stress of S_y= 235 MPa and ranges from 0.77 to 0.90S_u. Although the stress level is very high as a whole, all fatigue life is longer than 10^4 cycles corresponding to the lower limit of high cycle fatigue region, indicating that the copper film tested may be said fatigue-resistant. The slopes of *S-N* curves range only from -0.09 to -0.10 and are hardly influenced by the mean stress. Fig. 5(b) shows the data of the maximum stress S_{max} versus life. Irrespective of mean stress, fatigue life can be well represented by the maximum stress S_{max}. These results are different from the result of Park et al. [15] that fatigue life can be well represented by the modified Goodman equation rather than the maximum stress.

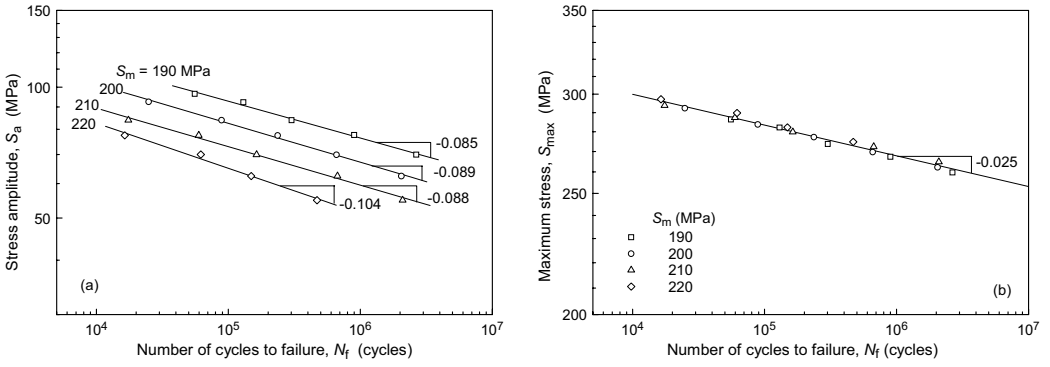

Fig. 5 (a) S_a-N_f, and (b) S_{max}-N_f curve

3.2.2. Cyclic deformation behavior

Fig. 6(a) shows variations of load-displacement curves with loading cycles. The load-displacement curve shifts in the positive direction of displacement with increasing number of cycles, indicating that the ratcheting occurs, and also the hysteresis loop representing the cyclic plastic deformation can be found in the curve. It is important for discussing fatigue of the testing material to precisely measure the cyclic plastic strain and ratcheting strain. However, as can be seen from the load-displacement curve in Fig. 6(a), since the cyclic plastic strain is very small compared with the cyclic elastic strain, it is difficult to accurately measure the plastic strain directly from the load-displacement curve. This difficulty can be solved by measuring the plastic strain separately from the elastic strain [19]. The plastic strain signal can be obtained by subtracting the output of load cell (proportional to the elastic strain) from the output of extensometer through the subtraction circuit, as illustrated in Figs. 7(a) and (b). In particular, by making the subtraction analogously rather than digitally in a computer, the differential signal can be thereafter amplified sufficiently to measure the plastic strain with very high precision. Separate measurement of the plastic strain is also important in using the specimen where the equivalent gage length is varied depending on whether elastic or plastic deformation. In this study, the plastic strain as small as 0.001 % could be measured.

Fig. 6(b) shows examples of load versus differential displacement (or stress–plastic strain) curves corresponding to Fig. 6(a). With load cycling, the mean plastic strain $\varepsilon_{p,mean}$, in other words, the so-called ratcheting strain, increases greatly. For convenience, the mean plastic strain $\varepsilon_{p,mean}$ will be hereafter referred to as the monotonic plastic strain. The cyclic plastic strain range $\Delta\varepsilon_p$ also increases, but the linear elastic portion of the load-differential displacement hysteresis loop gradually reduces to disappear in the late stages of life. This means that the material behaves almost wholly nonlinearly, particularly in the latter portions of life.

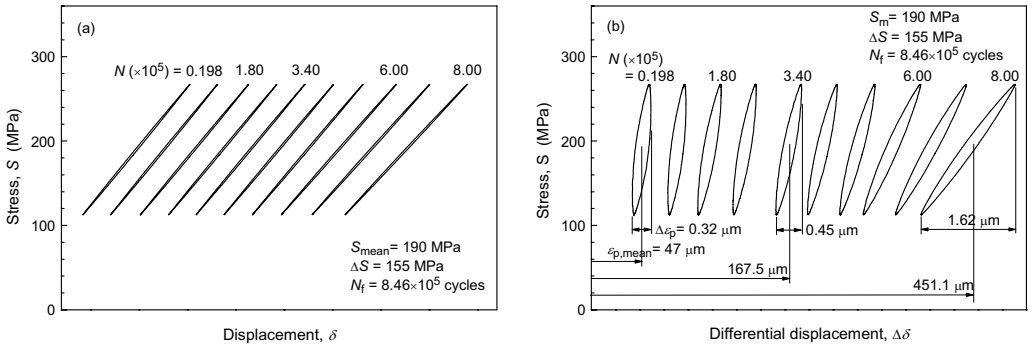

Fig. 6 Variations of (a) load-displacement curves and (b) load-differential displacement curves with loading cycles

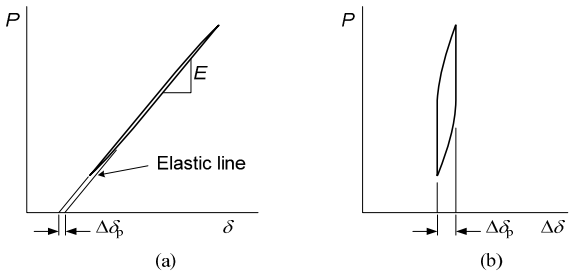

Fig. 7 (a) Load-displacement and (b) load-differential displacement curve

Fig. 8 shows examples of the cyclic plastic strain range $\Delta\varepsilon_p$ and the monotonic plastic strain $\varepsilon_{p,mean}$ curves against the number of cycles. All curves are similar to the conventional creep curve which consists of the three stages, namely, primary, steady-state and tertiary ones. The cyclic plastic strain range $\Delta\varepsilon_p$ varies only for small ranges from

about 0.01% at the initial stage to the value less than 0.1% at fracture, while the monotonic plastic strain $\varepsilon_{p,mean}$ varies from 1% to about 10%. The monotonic plastic strain $\varepsilon_{p,mean}$ is nearly ten times larger than the cyclic plastic strain range $\Delta\varepsilon_p$. In Fig. 9, the cyclic plastic strain range and the monotonic plastic strain at fracture, $\Delta\varepsilon_{p,fracture}$ and $\varepsilon_{pmean,fracture}$, are represented against the fatigue life N_f. In the $\Delta\varepsilon_{p,fracture}$-$N_f$ plot, the mean stress effect still remains. These results indicate that fatigue life can be hardly represented in terms of cyclic plastic strain. On the other hand, the value of $\varepsilon_{pmean,fracture}$ is nearly constant around 9.43%, irrespective of mean stress. This result implies that the copper film used in this study fails when the monotonic plastic strain ε_{pmean} reaches a limited value, $\varepsilon_{pmean,fracture}$ and consequently, also infers that the value of ε_{pmean} may be utilized as an indicator of damage.

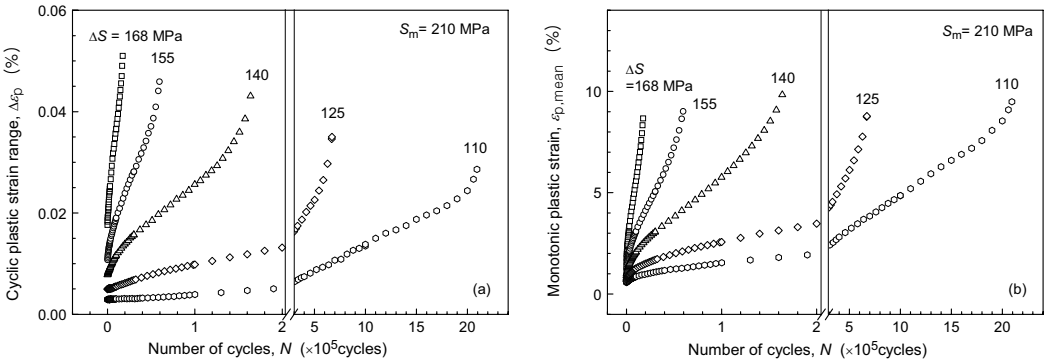

Fig. 8 Variations of (a) cyclic plastic strain range and (b) monotonic plastic strain

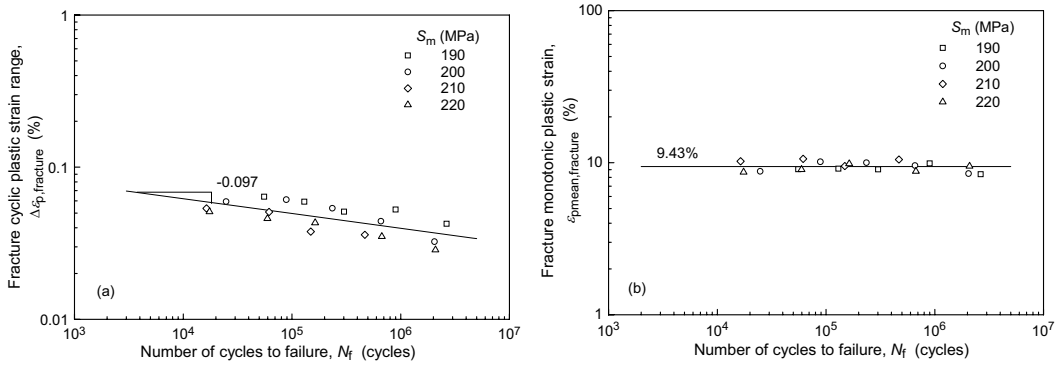

Fig. 9 Cyclic plastic strain range and monotonic plastic strain at fracture vs. life

3.3. Prediction of the monotonic plastic strain curve

Fig. 10(a) shows a typical example of the normalized monotonic plastic strain rate vs. normalized number of cycles curves, $(d\varepsilon_{p,mean}/dN)_{normalized}$-$N/N_f$, obtained from the monotonic plastic strain curve shown in Fig. 8(b), where both axes are normalized by using the maximum monotonic plastic strain rate $(d\varepsilon_{p,mean}/dN)_{max}$ and the fatigue life N_f. The strain rate curve shown in Fig. 10(a) is similar to the failure rate curve which can be represented by using the Weibull distribution [20] as follows

$$d\varepsilon_{p,mean} / dN = mN^{m-1} / \xi^m , \tag{8}$$

where m represents the shape parameter and ξ is the scale parameter. This implies that a monotonic plastic strain rate curve can be approximated by the Weibull distribution function and the monotonic plastic strain may be obtained from the approximated function. In order to obtain the two parameters, m and ξ, the monotonic plastic strain rate curve was appropriately divided into three regions as shown in Fig. 10(b), and then the curve for each region was approximated by using the Eq. (8). Fig. 10(b) shows an example of the approximated curves for three regions and the values of the two parameters obtained from the approximated curves were noted in the figure. Fig. 11 shows the calculated results of m and ξ for all experimental curves of the region 1 against the maximum stress $S_{\max}$. It can be seen from this figure that, for the region 1, the shape parameter m is nearly constant around $m = 0.5$, irrespective of $S_{\max}$, and the scale parameter ξ can be represented by the regression line of $\xi = (349.5/S_{\max})^{39.86}$. Similarly, the values of m and ξ for the other regions can be obtained, and the results for all regions are listed in Table 1. From Eq. (8), the monotonic plastic strain can be obtained as

$$\int_{\varepsilon_{\mathrm{pmean},i}}^{\varepsilon_{\mathrm{p,mean}}} d\varepsilon_{\mathrm{p,mean}} = \int_{N_i}^{N} mN^{m-1}/\xi^m dN\,, \tag{9}$$

$$\varepsilon_{\mathrm{p,mean}} = \varepsilon_{\mathrm{pmean},i} + (N^m - N_i^{m-1})/\xi^m\,. \tag{10}$$

From Eq. (10) and the parameters listed in Table 1, the monotonic plastic strain curves for three regions can be obtained as

$$\begin{aligned}
\varepsilon_{\mathrm{p,mean}} &= \varepsilon_{\mathrm{pmean},0} + (S_{\max}/349.5)^{19.93} N^{0.5} && \text{for region 1}\\
\varepsilon_{\mathrm{p,mean}} &= \varepsilon_{\mathrm{pmean},1} + (S_{\max}/363.7)^{39.07} (N - N_1) && \text{for region 2}\\
\varepsilon_{\mathrm{p,mean}} &= \varepsilon_{\mathrm{pmean},2} + (S_{\max}/373.9)^{110.91} (N^{2.8} - N_2^{2.8}) && \text{for region 3}
\end{aligned} \tag{11}$$

The values of N_1 and N_2, which represent number of cycles at the boundary between regions, were determined at the points where the slopes of the curve of region 1 and 3 equal to the slope of region 2, respectively. Fig. 12 shows examples of the predicted monotonic plastic strain curve, where the circle mark is the experimental data and the line represents the predicted result. It can be seen from this figure that the monotonic plastic strain curve is well predicted by using Eq. (11). The prediction results for all experimental data are represented in Fig. 13, where the solid lines represent the scatter band of factor 2 and the dashed lines represent scatter band of factor √2. The prediction life N_{pred} shown in Fig. 13 is the fatigue life corresponding to the monotonic plastic strain of $\varepsilon_{\mathrm{p,mean}}$= 9.43 % which is monotonic plastic strain at fracture, as shown in Fig. 11(a). It can be found from Fig. 13 that most prediction results are within the scatter band of factor √2, indicating that the prediction results by the Eq. (8) agree with the experimental data.

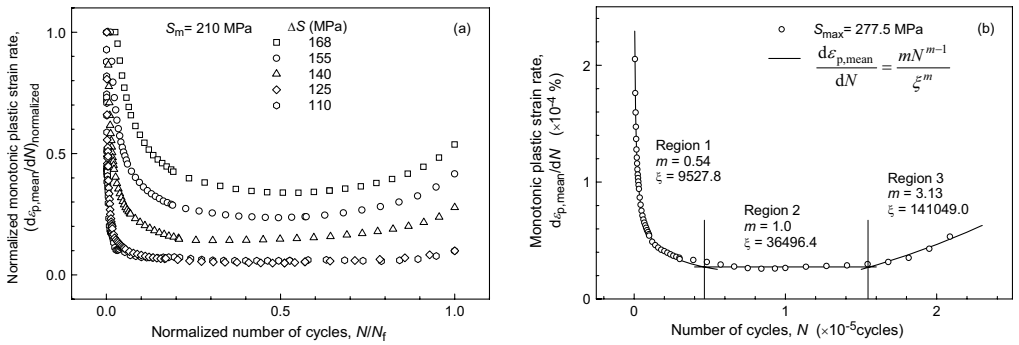

Fig. 10 The monotonic plastic strain rate curves

Table 1. The calculated results of m and ξ

	Region 1	2	3
m	0.5	1	2.8
ξ	$(349.5/S_{max})^{39.86}$	$(363.7/S_{max})^{39.07}$	$(373.9/S_{max})^{39.61}$

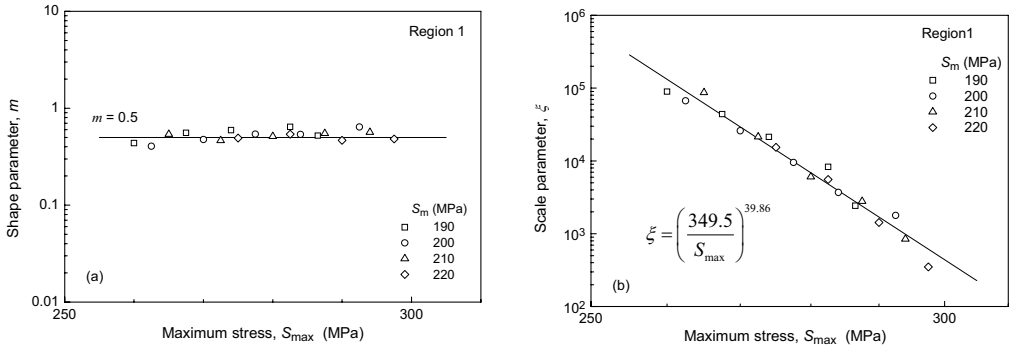

Fig. 11 The calculated results of m and ξ against the maximum stress S_{max} for the region 1

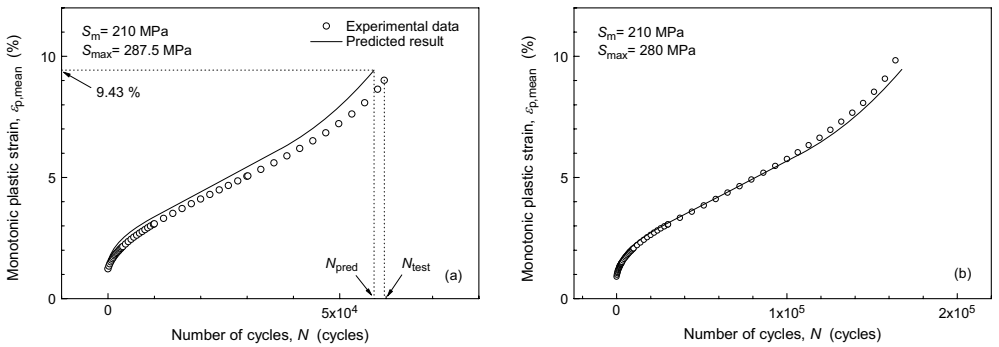

Fig. 12 Examples of the predicted monotonic plastic strain curve

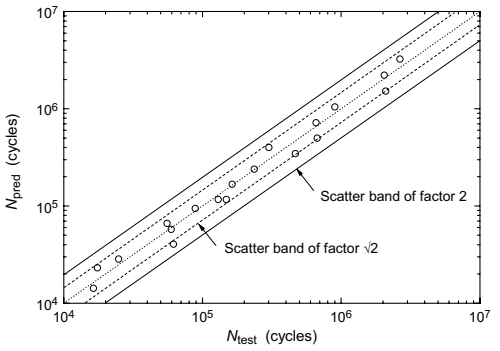

Fig. 13 Prediction results

4. Conclusion

In this study, plastic deformation behavior of electrodeposited copper films with thickness of 12 μm was investigated, using a fatigue testing system capable of performing load controlled tension-tension fatigue tests even for ductile thin films by using an electro-dynamic actuator. During the fatigue tests, cyclic plastic strain and ratcheting strain were measured continuously with high precision by using a home-made capacitance extensometer. Since the displacement gage is stable and its response is so fast, the deformation can be measured in real time during fatigue tests as well as tensile tests.

Although the level of stress applied is so high that all the maximum stress is greater than the yield stress, all fatigue life is longer than 10^4 cycles and belongs in high cycle fatigue region, implying that the copper film is fatigue resistant. The mean stress effect on fatigue life can be well described by the maximum stress. The cyclic plastic strain range and monotonic plastic strain increase with loading cycles and they are similar to the conventional creep curve. The monotonic plastic strain at fracture is nearly constant, irrespective of mean stress, indicating that the plastic strain can be used as an indicator of damage. Based on these results, a prediction method for the monotonic plastic strain is proposed. It could be found from the prediction results that the monotonic plastic strain can be well predicted within the scatter band of factor 2.

Acknowledgements

This research was supported by a Grant (2009K000180) from Center for Nanoscale Mechatronics and Manufacturing, one of the 21st Century Frontier Research Programs, which are supported by Ministry of Science and Technology, Korea.

References

[1] Connolley T, Mcchugh PE, Bruzzi M. *Fatigue Fract Eng Mater Struct* 2005;**28**:1119–52.
[2] Klein M, Hadrboletz A. Weiss B, Khatibi G, *Mater Sci Eng A* 2001;**319–321**:924–8.
[3] Haque MA, Saif MTA. *Scr Mater* 2002;47:863–7.
[4] Nilsson SG, Borrisé X, Montelius L. *Appl Phys Lett* 2004;**85**:3555–7.
[5] Angadi MA, Thanigaimani V. J *Mater Sci Lett 1994*;**13**:703–4.
[6] Ruud A, Josell D, Spaepen F, Greer AL. *J Mater Res* 1993;**8**:112–7.
[7] Keller RR, Phelps JM, Read DT. *Mater Sci Eng A* 1996;**214**: 42–52.
[8] Sharpe Jr WN, Yuan B, Edwardsb RL. J Microelectromech Syst 1997;**6**:193–9.
[9] Huang H, Spaepen F. *Acta Mater* 2000;**48**:3261–9.
[10] Read DT, Cheng YW, Keller RR, McColskey JD. *Scr Mater* 2001;**45**:583–9.
[11] Hong S, Weil R. *Thin Solid Films* 1996;**283**:175–81.
[12] Read DT. *Int J Fatigue* 1998;**20**:203–9.
[13] Allameh SM, Loua J, Kavishe F, Buchheit T, SoboyejoWO. *Mater Sci Eng A* 2004;371:256–66.
[14] Schwaiger R, Kraft O. *Acta Mater* 2003;**51**:195–206.
[15] Park JH, An JH, Kim YJ, Huh YH, Lee HJ, *Materialwiss Werkstofftech* 2008;**39**:187–92.
[16] Hwangbo Y, Song JH. *Mater Sci Eng A* 2010;**527**:2222–32.
[17] Kim CY, Song JH, Lee DY. *Int J Fatigue* 2009;**31**:736–42.
[18] Merchant HD, Khatibi G, Weiss B. *J Mater Sci* 2004;**39**:4157–70.
[19] Kikukawa M, Jono M, Kondo Y, Mikami S. *Trans JSME* 1982;**48**:1496–1540 (in Japanese).
[20] Song JH, Park JH. *Introduction to Reliability Engineering.* Seoul: Intervision; 2007 (in Korean).